

Submillimeter Test of the Gravitational Inverse-Square Law: A Search for “Large” Extra Dimensions

C. D. Hoyle, U. Schmidt, B. R. Heckel, E. G. Adelberger, J. H. Gundlach, D. J. Kapner, and H. E. Swanson

Department of Physics, University of Washington, Seattle, Washington 98195-1560

(Received 23 October 2000)

Motivated by higher-dimensional theories that predict new effects, we tested the gravitational $1/r^2$ law at separations ranging down to 218 μm using a 10-fold symmetric torsion pendulum and a rotating 10-fold symmetric attractor. We improved previous short-range constraints by up to a factor of 1000 and find no deviations from Newtonian physics.

DOI: 10.1103/PhysRevLett.86.1418

PACS numbers: 04.80.Cc

It is generally assumed that nonrelativistic gravity obeys an inverse-square law for all distances greater than the Planck length $R_P = \sqrt{G\hbar/c^3} = 1.6 \times 10^{-33}$ cm. However, the gravitational interaction has only been tested [1–7] with good precision for separations greater than 1 cm and, as summarized in Ref. [8], very little is known about gravity at length scales below a few mm. Recently theorists, using several different arguments, have suggested that the unexplored short-range regime of gravitation may hold profound surprises [9–12], i.e., that the gravitational interaction could display fundamentally new behavior in the mm regime.

Many of these arguments are based on the notion, intrinsic to string or M theory, of more than three spatial dimensions. To maintain consistency with a vast body of observations the extra dimensions must be “curled up” in very small regions, usually assumed to be comparable to R_P , or else hidden in some other way [13]. It has recently been noted [9,10] that the enormous discrepancy between natural mass scales of the standard model of particle physics ($M_{SM} \approx 1$ TeV) and of gravity (the Planck mass $M_P = \sqrt{\hbar c/G} = 1.2 \times 10^{16}$ TeV) could be eliminated if gravity propagates in *all* the space dimensions while the other fundamental interactions are constrained to the three familiar dimensions. This unification scenario requires that some of the extra dimensions have radii R^* that are large compared to R_P with

$$R^* = \frac{\hbar c}{M^* c^2} \left(\frac{M_P}{M^*} \right)^{2/n}, \quad (1)$$

where M^* is the unification scale (usually taken as M_{SM}) and n is the number of large extra dimensions. The scenario with $n = 1$ is ruled out by astronomical data. If there are two large extra dimensions, R^* must be about 1 mm, and the gravitational inverse-square law (which follows from Gauss’s law in three spatial dimensions) will turn into a $1/r^4$ law (Gauss’s law in five dimensions) at distances much smaller than R^* .

Other theoretical considerations also suggest that new effects may show up at short distances; string theories predict scalar particles (dilaton and moduli) that generate Yukawa interactions which could be seen in tests of

the $1/r^2$ law. If supersymmetry is broken at low energies these scalar particles would produce mm-scale effects [11,14]. Finally, there may be some significance to the observation [12] that the gravitational cosmological constant, $\Lambda \approx 3$ keV/cm³, deduced from distant Type-1A supernovae [15,16], corresponds to a length scale $\sqrt{\hbar c/\Lambda} \approx 0.1$ mm. These, and other, considerations suggest that the Newtonian gravitational potential should be replaced by a more general expression [17]

$$V(r) = -G \frac{m_1 m_2}{r} (1 + \alpha e^{-r/\lambda}). \quad (2)$$

The simplest scenario with two large extra dimensions predicts $\lambda = R^*$ and $\alpha = 3$ or $\alpha = 4$ for compactification on a 2-sphere or 2-torus, respectively [17], while dilaton and moduli exchange could produce forces with α as large as 10^5 for Yukawa ranges $\lambda \sim 0.1$ mm [11].

This Letter reports results of a test of gravitational inverse-square law at length scales well below 1 mm. Our instrument is shown in Fig. 1.

An 82 cm-long, 20- μm -diameter tungsten fiber, hanging from an x - y - z - ϑ stage, supported a torsion pendulum with 10-fold rotational symmetry. The pendulum was placed above a 10-fold symmetric attractor that rotated slowly about the vertical axis of the pendulum. The active component of the pendulum was a 2.002-mm-thick aluminum annulus containing ten equally spaced 9.528-mm-diameter holes, centered on a 55.33-mm-diameter circle. The active component of the attractor consisted of two coaxial copper disks. The 1.846-mm-thick upper disk had ten 9.535-mm-diameter holes centered on a 55.31-mm circle, while the 7.825-mm-thick lower disk had ten 12.690-mm-diameter holes centered on a 55.33-mm circle. The holes in the lower disk were rotated azimuthally by 18° compared to the upper holes; this geometry substantially reduced the signal from Newtonian gravity but had little effect on a short-range signal.

We measured the torque on the pendulum, produced by the interactions between the holes in the attractor and the pendulum, for pendulum-to-attractor vertical separations, ζ , down to 218 μm . Because of the 10-fold rotational symmetry of the instrument this torque varied

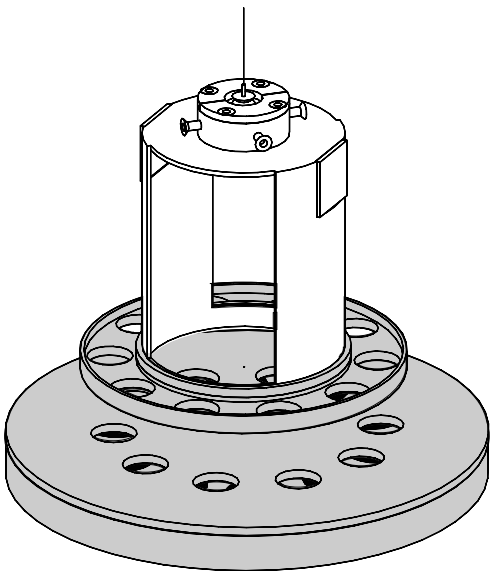


FIG. 1. Scale drawing of the torsion pendulum and rotating attractor. The active components are shaded. For clarity, we show an unrealistically large 1.5 cm vertical separation between pendulum and attractor, and omit the BeCu membrane and the attractor drive mechanism. The four horizontal screws were adjusted to make the pendulum precisely level.

at 10 times the attractor rotation frequency ω . Spurious torques from electrical forces were minimized by placing a tightly stretched, 11.4-cm-diameter, 20- μm -thick beryllium-copper membrane between the attractor and pendulum, 48 μm above the upper surface of the attractor. The pendulum, mirrors, membrane, and upper surface of the attractor were coated with gold, and the pendulum and membrane were surrounded by a gold-plated copper enclosure. Crucial dimensions of the pendulum and attractor were good to $\pm 2.5 \mu\text{m}$, and the membrane, which had a mirrorlike finish, was flat to within $\pm 15 \mu\text{m}$.

The torque on the pendulum was inferred from the pendulum twist angle, θ , which we measured by reflecting an autocollimator light beam twice from either of two flat mirrors mounted on the pendulum. The attractor rotation period, τ_A , was set to $17\tau_0$, where $\tau_0 = 2\pi/\omega_0 \approx 399.6$ s was the period of the pendulum's free torsional oscillations. The attractor angle, $\phi = \omega t$, and signals from the autocollimator, the ion-pump pressure gauge, a 2-axis electronic level on the instrument, and eight temperature sensors were digitized at regular intervals, typically $\tau_D = \tau_0/36$, and stored in a small computer. Data, acquired continuously, were broken into "cuts," each of which had exactly two oscillations of the 10ω signal. For each "cut," the filtered [18] pendulum twist $\tilde{\theta}$ as a function of ϕ was fitted with

$$\tilde{\theta}(\phi) = \sum_n [b_n \sin n\phi + c_n \cos n\phi] + \sum_{m=0}^2 d_m P_m, \quad (3)$$

where the first sum ran over $n = 1, 3, 10, 20$, and 30. The floating $n = 10, 20$, and 30 terms yielded the fundamen-

tal and leading harmonics of the torque signal; the small $n = 1$ and $n = 3$ terms were fixed by fitting data covering one complete revolution of the attractor. The $n = 3$ coefficients accounted for the three-fold symmetry of the attractor drive system, and the $n = 1$ coefficients, typically consistent with zero, were used for diagnostic purposes. The d_1 and d_2 polynomial coefficients allowed for the slow unwinding of our torsion fiber ($\leq 0.2 \mu\text{rad/h}$).

Figure 2 shows a typical segment of fitted autocollimator data.

The resulting $n = 10, 20$, and 30 torques are

$$T_n = I |(\tilde{b}_n + i\tilde{c}_n)(\omega_0^2 - n^2\omega^2 + 2i\gamma n\omega)| \times \sec\left(\frac{\pi n\omega}{2\omega_0}\right), \quad (4)$$

where $I = 128.4 \text{ g cm}^2$ is the calculated rotational inertia of the pendulum, the superscript tildes on the b and c coefficients indicate corrections for electronic time constants (see Ref. [4]), and the damping coefficient $\gamma \approx 5 \times 10^{-6} \text{ s}^{-1}$ is the reciprocal of the observed decay time of the free torsional amplitude. We measured ω_0 for each data point and found it was constant to within 0.3%.

Our data sets consisted of the T_{10} , T_{20} , and T_{30} torques as functions of separation. Clearly, compared to Newtonian gravity, a short-range $1/r^2$ -violating force will have both a higher harmonic content and a stronger dependence on ζ . Data taken at ζ 's ranging from 218 μm to 10.78 mm and at several horizontal displacements x and y , were compared to calculations of the signals expected from the potential of Eq. (2). The expected Newtonian (Yukawa) twists were computed to a precision better than $0.1(0.3\alpha)$ nrad while a typical measured point had a statistical error of 8 nrad. We found analytic solutions for four of the Newtonian integrals and two of the Yukawa integrals and evaluated the remaining integrals numerically. Figure 3 shows the T_{10} , T_{20} , and T_{30} torques together with the Newtonian predictions. We fitted these

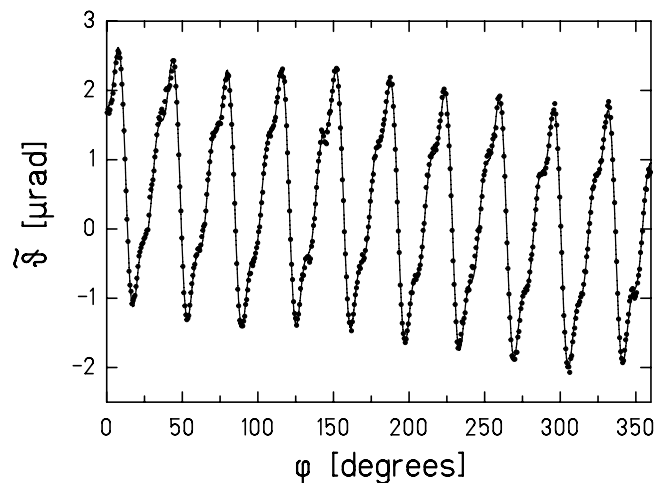


FIG. 2. Autocollimator data for one complete revolution of the attractor, taken at $\zeta = 237 \mu\text{m}$. The curve is a fit to Eq. (3).

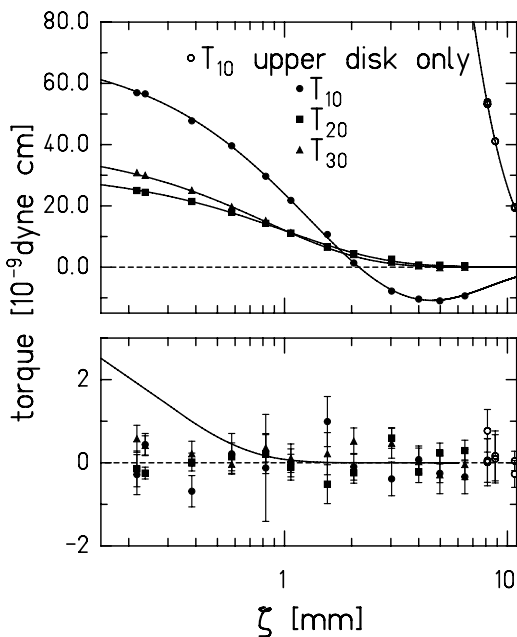


FIG. 3. T_{10} , T_{20} , and T_{30} torques, and the 10ω torque from the upper attractor alone. Each point contains at least 36 individual measurements; the 1σ error bars are derived from the scatter of the individual measurements. The upper panel shows the measured torques; the solid lines are the Newtonian prediction. The T_{10} sign change at $z = 2.2$ mm is due to cancellation from the bottom set of holes. The lower panel displays the Newtonian fit residuals; the solid curve shows the effect on T_{10} of an interaction with $\alpha = 3$ and $\lambda = 250 \mu\text{m}$.

data, for a series of λ values, with the physics parameter α and four constrained and two unconstrained parameters describing the instrument. The constrained instrumental parameters (the gap $\epsilon = 10 \pm 10 \mu\text{m}$ between the two attractor disks, the ratio of the “masses” of the holes in the upper and lower disks $\rho = 0.1329 \pm 0.0001$, a factor $f = 1.000 \pm 0.003$ representing the uncertainties in the torque scale and the “mass” of the pendulum holes, and $z_0 = 910 \pm 5 \mu\text{m}$ the z -micrometer reading at $\zeta = 0$) were determined by auxiliary measurements described below. The unconstrained instrumental parameters x_0 and y_0 were the centered values of x and y micrometers. In all cases, the best-fit values of the constrained experimental parameters agreed with their nominal values; the average and maximum deviations were 1.3σ and 1.9σ , respectively. Our data are well described by Newtonian gravity with a χ^2 per degree of freedom of 1.03 with a probability of 41%. The resulting constraints on new physics of the form given in Eq. (2) are shown in Fig. 4; scenarios with $\alpha \geq 3$ are excluded at 95% confidence for $\lambda \geq 190 \mu\text{m}$.

Accurate alignment and control of the pendulum and attractor geometry and precise calibrations were essential in this experiment.

The attractor geometry parameters were determined using a measuring microscope, and the “masses” of the pendulum and attractor holes were computed from their

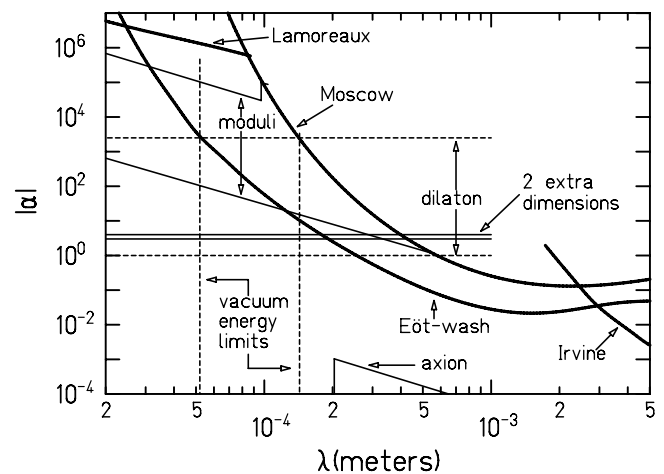


FIG. 4. 95% confidence upper limits on $1/r^2$ -law violating interactions of the form given by Eq. (2). The region excluded by previous work [2,3,20] lies above the heavy lines labeled Irvine, Moscow and Lamoreaux, respectively. The data in Fig. 3 imply the constraint shown by the heavy line labeled Eöt-wash. Constraints from previous experiments and the theoretical predictions are adapted from Ref. [8], except for the dilaton prediction which is from Ref. [14].

dimensions and the measured densities of the active components of the pendulum and attractor. The torque scale was calibrated gravitationally. Two small aluminum spheres, inserted into diametrically opposite holes in a similar pendulum annulus, gave it a known q_{22} spherical multipole moment. A Q_{22} attractor moment was created by two bronze spheres, centered on the torsion pendulum and separated by 27.965 cm. These spheres were rotated around the pendulum axis by a turntable to produce a $(4.010 \pm 0.001) \times 10^{-7}$ dyne-cm 2ω torque on the pendulum.

The z -micrometer setting at vanishing vertical pendulum-to-membrane separation was inferred from the capacitance between the pendulum and the membrane. (The membrane and the upper fiber attachment, which were normally grounded to the vacuum can, were electrically isolated for these measurements.) We fitted the capacitance as a function of the z -micrometer setting (see Fig. 5), with an expression for a plane electrode parallel to an infinite plate [19]. (The function, which contained a leading-order expression for the fringing fields, was integrated over the pendulum’s sinusoidal “bounce” motion.) The fixed vertical separation between the membrane and attractor ($48 \pm 3 \mu\text{m}$) and their parallelism (misalignment ≤ 0.2 mrad) were measured using depth micrometers and a special jig that could be substituted for the membrane. A capacitive measurement gave a consistent value for this separation. The peak-to-peak vertical runout and “wobble” as the attractor rotated were ≤ 1.3 and $\leq 5 \mu\text{m}$, respectively.

The pendulum plane was adjusted to be horizontal to < 0.2 mrad by temporarily replacing the normal membrane

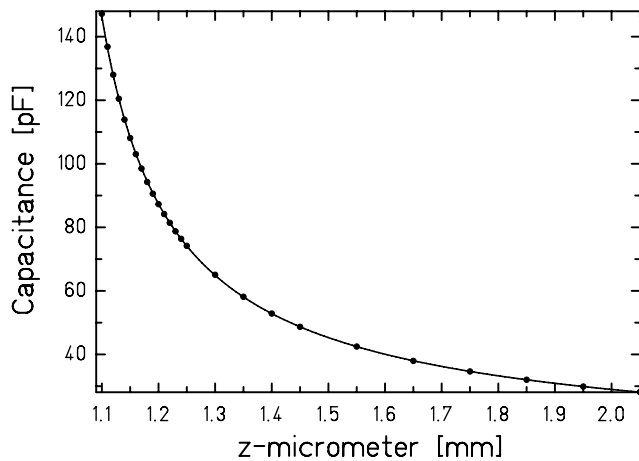


FIG. 5. Capacitance measurements of the separation. The horizontal axis is the reading of the z micrometer. The fit indicated that the pendulum would touch the screen at $z = 978 \pm 3 \mu\text{m}$.

with two isolated semicircular copper disks that, together with the pendulum, formed a differential capacitor. We then monitored the 1ω differential capacitance signal as ϑ was rotated at a steady rate and adjusted the pendulum's small trim screws (shown in Fig. 1) to minimize this signal. (The leveling precision was limited by the $\pm 74 \mu\text{m}$ horizontal runout of the fiber as ϑ was rotated.) The semicircular disks were removed and the reinstalled membrane was made parallel to the pendulum (to within <0.1 mrad) by tilting the entire instrument and finding the angle that gave the smallest capacitance for a fixed value of z . Then the x and y micrometers were adjusted to recenter the pendulum on the attractor by maximizing the 10ω , 20ω , and 30ω signals.

We checked that likely nongravitational sources of systematic error had negligible effects on our results. The attractor drive mechanism was largely nonmagnetic; the amplitude of magnetic field variations at the site of the pendulum was $\leq 0.6 \mu\text{G}$ at the signal frequency. The measured sensitivity of the pendulum to magnetic field variations at the signal frequency was 57 nrad/mG, corresponding to a magnetic systematic error of 0.03 nrad. The energy dissipated in the attractor motor warmed the attractor slightly. A five-fold increase in the motor's temperature rise, produced by attaching heat-dissipating resistors to the motor housing, changed \tilde{b}_{10} and \tilde{b}_{20} by 17 ± 11 nrad and -4 ± 9 nrad, respectively. We found that an overall 98 mK change of the instrument's temperature changed the equilibrium twist of the fiber by $1.17 \mu\text{rad}$. During normal operation, none of the sensors on the instrument had temperature variations at the 10ω signal frequency that exceeded $100 \mu\text{K}$, indicating that spurious signals from temperature variations were ≤ 1 nrad. When the attractor rotation period was changed from $7\tau_0$ to $43\tau_0$ (the normal period was $17\tau_0$),

\tilde{b}_{10} and \tilde{b}_{20} were unchanged to within 5 ± 15 nrad and 11 ± 31 nrad, respectively.

Our results, interpreted in the simplest unification scenario with two equal large extra dimensions, imply a unification scale given in Eq. (1) of $M^* \geq 3.5$ TeV. We are now preparing a second-generation experiment with a different pendulum and attractor that should provide higher precision and better sensitivity at small λ .

We thank Professor David Kaplan and Professor Ann Nelson for helpful discussions, and Nathan Collins, Angela Kopp, and Deb Spain for assistance with the experiment. This work was supported primarily by the NSF (Grant No. PHY-9970987) and secondarily by the DOE.

-
- [1] D. E. Krause and E. Fischbach, hep-ph/9912276.
 - [2] J. K. Hoskins, R. D. Newman, R. Spero, and J. Schultz, Phys. Rev. D **32**, 3084 (1985).
 - [3] V. P. Mitrofanov and O. I. Ponomareva, Sov. Phys. JETP **67**, 1963 (1988).
 - [4] G. L. Smith, C. D. Hoyle, J. H. Gundlach, E. G. Adelberger, B. R. Heckel, and H. E. Swanson, Phys. Rev. D **61**, 022001 (2000).
 - [5] Y. Su, B. R. Heckel, E. G. Adelberger, J. H. Gundlach, M. Harris, G. L. Smith, and H. E. Swanson, Phys. Rev. D **50**, 3614 (1994).
 - [6] S. Baeßler, B. R. Heckel, E. G. Adelberger, J. H. Gundlach, U. Schmidt, and H. E. Swanson, Phys. Rev. Lett. **83**, 3585 (1999).
 - [7] C. M. Will, in *The Confrontation between General Relativity and Experiment*, edited by M. C. Bento *et al.* (World Scientific, Singapore, 1993), p. 183.
 - [8] G. C. Long, H. Chang, and J. Price, Nucl. Phys. **B529**, 23 (1999).
 - [9] N. Arkani-Hamed, S. Dimopoulos, and G. Dvali, Phys. Lett. B **429**, 263 (1998).
 - [10] N. Arkani-Hamed, S. Dimopoulos, G. Dvali, and N. Kaloper, Phys. Rev. Lett. **84**, 586 (2000).
 - [11] S. Dimopoulos and G. Guidice, Phys. Lett. B **379**, 105 (1996).
 - [12] R. Sundrum, J. High Energy Phys. **9907**, 001 (1999).
 - [13] L. Randall and R. Sundrum, Phys. Rev. Lett. **83**, 4690 (1999).
 - [14] D. B. Kaplan and M. B. Wise, J. High Energy Phys. **0008**, 037 (2000).
 - [15] A. G. Riess *et al.*, Astron. J. **116**, 1009 (1998).
 - [16] S. Perlmutter *et al.*, Astrophys. J. **517**, 565 (1999).
 - [17] E. G. Floratos and G. K. Leontaris, Phys. Lett. B **465**, 95 (1999); A. Kehagias and K. Sfetsos, *ibid.* **472**, 39 (2000) [Our Eq. (2) is valid for extra dimensions of size R^* as long as $r \geq R^*$.]
 - [18] A simple digital filter suppressed free torsion oscillations as described in Ref. [4].
 - [19] L. D. Landau, E. M. Lifshitz and L. P. Pitaevskii, *Electrodynamics of Continuous Media* (Pergamon Press, New York, 1984), 2nd ed., p. 18.
 - [20] S. K. Lamoreaux, Phys. Rev. Lett. **78**, 5 (1997).